THE JOURNAL OF PHYSICAL CHEMISTRY C
A JOURNAL OF THE AMERICAN CHEMICAL SOCIETY

pubs.acs.org/JPCC

Article

Assembly Control at a Low Péclet Number in Ultracentrifugation for Uniformly Sized Nanoparticles

Xufeng Xu, Baohu Wu, Helmut Cölfen,* and Gijsbertus de With*

Cite This: *J. Phys. Chem. C* 2021, 125, 8752–8758

Read Online

ACCESS | Metrics & More | Article Recommendations | Supporting Information

ABSTRACT: The intrinsic high diffusion rate of colloids at low Péclet number results in an extremely fast crystallization process and instant formation of colloidal crystals, even at an ultracentrifugal field of extremely high intensity. By introducing a small number of clusters in sedimention, it should be possible to slow down the crystallization process, thus making the assembly order tunable in preparative ultracentrifugation experiments. Here, we used sodium dodecyl sulfate-stabilized polystyrene nanoparticles (with a size dispersity of 1.07) dispersed in a solution of high ionic strength. Sedimentation and assembly of these nanoparticles were done using preparative ultracentrifugation at various angular velocities. The sedimentation process was also analyzed in situ by analytical ultracentrifugation in real time. By creating as low as 3% of clusters into these nearly uniformly sized polystyrene nanoparticle dispersions during the sedimentation process, the superstructure order becomes easily tunable between glassy and crystalline. Theoretical calculations complemented the experiments to explain the mechanism of cluster formation in sedimentation. This work provides a novel methodology to produce superstructures with a tunable packing order for colloids at low Péclet number.

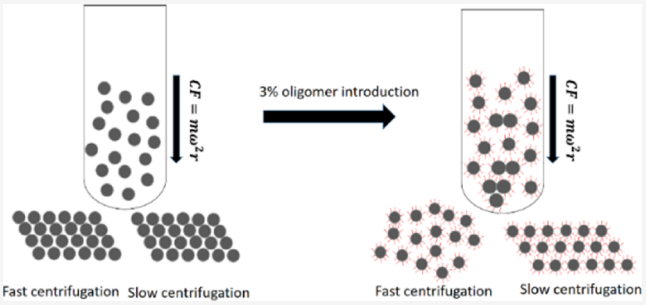

1. INTRODUCTION

Colloidal particles are promising building blocks for the fabrication of micro-, meso-, and macroscale materials with controlled properties and functions.[1,2] For example, colloidal particle-based materials are widely used for carbon dioxide capture,[3] as catalyst supports[4] and for fuel cell construction.[5] Among these, the assembly of monodisperse colloidal particles[6,7] represents the simplest case. There are currently a wide variety of bottom-up assembly methods available including controlled evaporation, vertical deposition, spin coating, and so on.[7,8] Among these methods, sedimentation-induced assembly is a fast and versatile approach[9,10] and the superstructure order is well described by the Péclet number (Pe):[11] a low value of Pe leads to a crystalline structure, while a high Pe value leads to a glassy one. In principle, the Péclet number is the ratio of the initial rate of sedimentation ($\Delta\rho g^* a^2$) and the crystallization rate (kT/a^2), as described in eq 1

$$Pe = \Delta\rho g^* a^4/kT \tag{1}$$

where $\Delta\rho$ is the density difference between the colloids and the solvent, g^* is the force due to the centrifugal field, which can be calculated from revolutions per minute (RPM) and the distance from the rotation center to the center of the sample (r) using $g^* = r \times \mathrm{RPM}^2$, and a is the particle radius. As usual, k and T denote Boltzmann's constant and temperature, respectively. From eq 1, it is clear that Pe is proportional to a^4, which means that the possibility of forming a glassy structure increases rapidly with particle size. Accordingly, the tuning of the superstructure order was shown very successfully for micrometer-sized colloids.[10,12] However, for nanosized colloids, fast sedimentation was tested as well and shown to be completely unsuccessful to realize a glassy structure.[13,14] As shown in Figure 1A–C, only a crystalline structure was formed even when Pe increased to 0.1 with a centrifugal field as strong as 153 900g (g is the acceleration of gravity). The reason is that for monodisperse nanoparticles, the crystal nucleation and growth rate are much faster than the sedimentation rate during ultracentrifugation,[15,16] which is demonstrated by a small Pe value. In this paper, we show that the assembly order for monodisperse colloidal particles, that is whether crystallization occurs or not, can be simply controlled in a centrifugal field. The strategy used is the introduction of a tiny amount (as low as 3%) of clusters during the sedimentation process. The presence of this small amount of clusters slightly increases the size dispersity of the nanoparticles in dispersion, which in turn raises the crystal nucleation barrier significantly.[15] This leads to

Received: January 7, 2021
Revised: March 31, 2021
Published: April 15, 2021

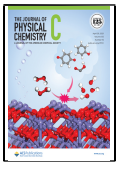

https://doi.org/10.1021/acs.jpcc.1c00143
J. Phys. Chem. C 2021, 125, 8752–8758

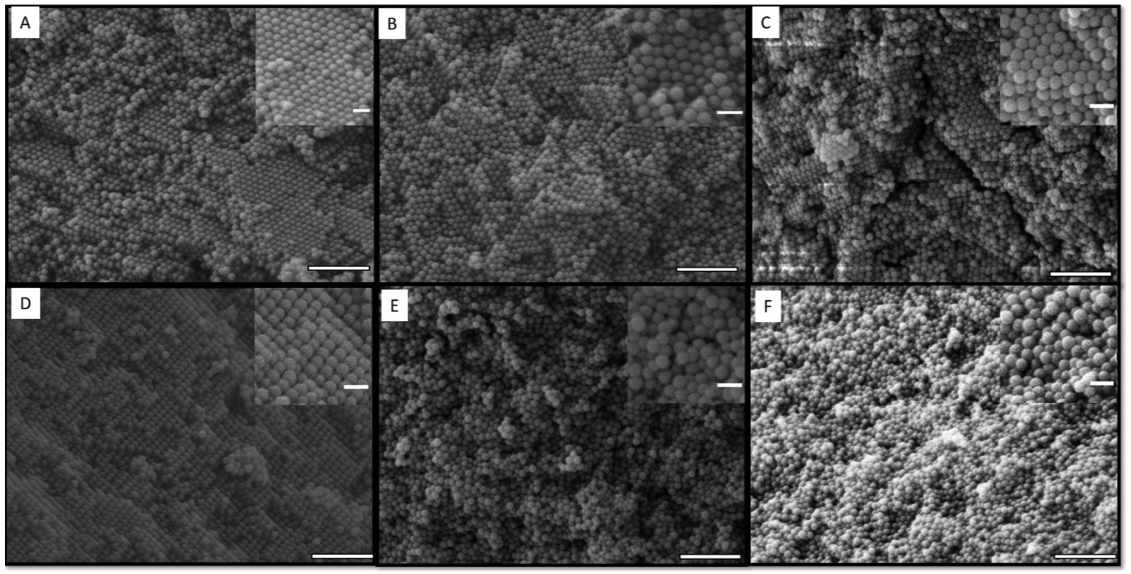

Figure 1. Scanning electron microscopy (SEM) images of colloidal assembly structures after complete sedimentation of charge-stabilized PS nanoparticles in water at (A) 12 000 (17 100*g*), (B) 24 000 (68 400*g*), and (C) 36 000 rpm (153 900*g*) and of sodium dodecyl sulfate (SDS)-stabilized PS nanoparticles in pH 2 buffer at (D) 12 000 (17 100*g*), (E) 24 000 (68 400*g*), and (F) 36 000 (153 900*g*). The scale bar is 1 μm. The insets are the magnified views of nearly flat areas for each image, for which the scale bar is 200 nm. From these images, a (fast) Fourier transform (FFT) and a radial distribution function (RDF) can be calculated to analyze the ordering of the structure (see the Supporting Information (SI 4)). For pure PS added to pH 2 buffer, immediately, visually observable precipitation occurs, and therefore follow-up centrifugation was omitted.

a delayed crystallization process,[17] which makes it possible for monodisperse colloids to form a glassy superstructure in a strong centrifugal field. The method provides a novel way to control the assembly order for monodisperse nanoparticles.

2. MATERIALS AND METHODS

2.1. Preparation of Sterically Stabilized Polystyrene Nanoparticles. A 10 vol % stock polystyrene (PS) bead suspension (radius ca. 50 nm) was bought from Sigma-Aldrich. The suspension was purified by dialysis against Milli-Q water for several days until the conductivity of the dialysis water did not change. An appropriate amount of sodium dodecyl sulfate (SDS) was dissolved in the PS suspension to obtain a final concentration of 0.8 mM. The suspension was then diluted 10 times by pH 2 buffer (0.08 M KCl and 0.02 M HCl mixture) to make a 1 vol % PS suspension for further use.

To estimate the surface coverage, we use the data given by Turner et al.[18] obtained by neutron reflection (NR) and infrared measurements over a range of SDS concentrations using PS as a substrate in water. At a critical micelle concentration (cmc) of 8 mM, the area per SDS was estimated as 42 Å^2. Moreover, the surface coverage was given as 4.0 μmol m^{-2} at the cmc and 1.7 μmol m^{-2} at 0.8 mM. Hence, in our case (0.8 mM SDS), the area per SDS is about (4.0/1.7)42 Å^2 = 100 Å^2 or ca. 1 SDS per 100 Å^2 (a similar value results from an estimate using the PS bead size and SDS concentration assuming that all of the SDS molecules adsorb on the PS surface).

The suspension was diluted to an appropriate concentration for dynamic light scattering and ζ-potential measurements. The ζ measurements were conducted using a Malvern Zetasizer Nano ZSP. The conversion from electrophoretic mobility to ζ-potential was done by employing the Henry equation using the Smoluchowski approximation as appropriate for aqueous dispersions.[19]

2.2. Detailed Sample Preparation for SEM Characterization. For a typical preparative ultracentrifugation experiment, a PS suspension (1 vol %, 480 μL) was filled into a centrifugal tube (5 mL, an open-top thin-wall polypropylene tube). The tube was put into a swing-out rotor (Beckman SW 55 Ti) and then the rotor was put inside an ultracentrifuge (L-70, Beckman instruments). After centrifugation at 20 °C for 22 min at 12 000 rpm (to realize complete sedimentation), the supernatant was removed before the centrifuge tube was frozen in liquid nitrogen. The frozen sample was connected to a freeze dryer typically for 1−2 days to completely dry the sample. After that, the dried sample was cut into pieces by a razor blade before loading on a SEM stub for SEM characterization. Using this procedure, the nanoparticle packing order inside the sediment can be observed well. At least five images were taken at random positions to obtain a representative picture of the nanoparticle ordering. To confirm that the nanoparticle ordering so observed was indeed representative, this whole experiment was repeated at least three times.

3. RESULTS AND DISCUSSION

3.1. Characterization of Sterically Stabilized Colloids. The dispersion of monodisperse polystyrene (PS) beads (radius $a \cong 50$ nm) was first purified by dialysis and then mixed with a small amount of sodium dodecyl sulfate (SDS) (0.8 mM) to obtain sterically stabilized nanoparticles.[18] The driving force for the adsorption of SDS on the PS surface is mainly hydrophobic attraction.[20−22] The surface area per SDS molecule on PS beads with a = 55 nm was measured by Piirma and Chen[21] to be 47 Å^2 using soap titration. A similar value of 46 Å^2 was obtained by Nodehi et al. for SDS on PS beads with a = 48 nm[23] using conductometric titrations. In our case, the area per SDS is ca. 1 SDS per 100 Å^2 as calculated above, a value about twice that for the maximum coverage. Speaking of the conformation of SDS on the PS surface, stretched-out chains of SDS may be present in our case due to (1)

https://doi.org/10.1021/acs.jpcc.1c00143
J. Phys. Chem. C 2021, 125, 8752−8758

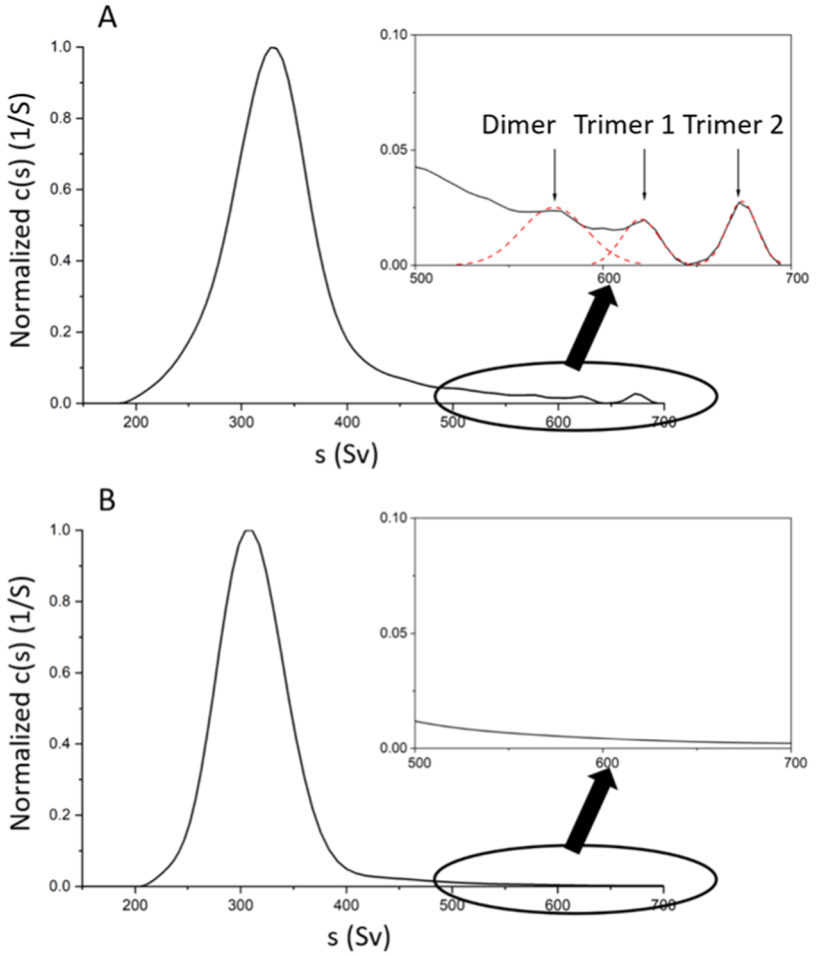

Figure 2. Sedimentation coefficient distribution using the $c(s)$ model in the software Sedfit[26] for SDS-stabilized PS nanoparticles in pH 2 buffer (A) and for charge-stabilized PS nanoparticles in water (B) of 1 wt % and at 15 000 rpm (17 100g) by AUC. The inset figures zoom in the range from 500 to 700 Sv and show whether there is the presence of clusters. By the Gaussian fitting (red dashed curves) of the cluster peaks, the amount of the clusters was estimated to be 3%.

electrostatic repulsion between the negatively charged sulfate group present both in SDS and on the PS particle surface and (2) favorable interactions between the sulfate head group of SDS and the aqueous solution and (3) entropy penalty,[20,22] although hydrophobic interaction tends to push SDS lying flat. A molecular dynamic (MD) simulation[20] indicates that for a coverage of 0.01 $Å^{-2}$ (or 0.48 mg m^{-2}) as present experimentally, the SDS molecules do stretch out on the surface of PS beads. This is also consistent with small-angle X-ray scattering (SAXS) data[24] and neutron reflection (NR) combined with attenuated total reflection infrared (ATR-IR) data of SDS adsorbed on PS in water.[18] Also, our dynamic light scattering (DLS) data, indicating a change in the number-weighted average diameter from 87.4 to 88.7 nm upon SDS adsorption (see Table S1), support a stretched-out conformation. Furthermore, SAXS showed an SDS shell of ca. 1 nm thickness on PS beads.[24] This agrees well with a more precise value of ca. 1.2 nm at a coverage of 0.01 $Å^{-2}$, as measured by neutron reflection.[18] In our case, the SDS adsorption was confirmed by an increase of surface charge, measured by ζ-potential experiments and the thickness was estimated by DLS.[25] As shown in Table S1 in the SI 1, after 0.8 mM SDS was added, the particle diameter increased by ca. 2 nm, indicating that an SDS layer with a thickness of ca. 1 nm is present on the PS nanoparticles. To suppress the electrostatic repulsion between the negatively charged PS nanoparticles, the nanoparticles were dispersed in a high-ionic-strength buffer (0.1 M). Thus, in this case, the PS nanoparticles were stabilized by the surface-bound surfactants. DLS, very small angle neutron scattering (VSANS) (for details of the VSANS experiments, see SI 2) and analytical ultracentrifugation (AUC) (see Figures S1−S4) all showed that no aggregates were present in the dispersion. In this way, uniformly sized PS nanoparticle dispersions sterically stabilized with SDS and having a dispersity as low as 1.07 were prepared for further use (for a detailed comparison of size and dispersity obtained by different techniques, see SI 3).

3.2. Preparative and Analytical Ultracentrifugation. As can be seen from Figure 1A−C, charge-stabilized PS nanoparticles were not sensitive to the angular velocity change at all and only crystalline structures were formed. The reason is that the *Pe* value is still as low as 0.1, even when the angular velocity was increased to as high as 36 000 rpm (centrifugal force $g^* \approx 153\,900g$, as the distance from the rotation center to the center of the sample is 105.5 mm using an SW 55 Ti rotor). In contrast, SDS-stabilized PS nanoparticles assembled into a crystalline structure at 12 000 rpm ($g^* \approx 17\,100g$), while they packed into a glassy structure at an angular velocity higher than 24 000 rpm ($g^* \geq 68\ 400g$), as shown in Figure 1D−F. A more quantitative analysis of the ordering of nanoparticles in

https://doi.org/10.1021/acs.jpcc.1c00143
J. Phys. Chem. C 2021, 125, 8752−8758

these images was made by calculating the associated fast Fourier transform (FFT) and radial distribution function (RDF), as discussed in detail in SI 4 (Figure S6A–F shows the corresponding radial distribution functions (RDFs) and Figures S6G–L represents the corresponding fast Fourier transforms (FFTs)). Thus, for colloids assembled at the same low *Pe* value, order control is easily realized for surfactant-stabilized colloids by tuning the sedimentation rate, while for charge-stabilized colloids, order control is not possible in the same angular velocity range. Analytical ultracentrifugation (AUC) employing Rayleigh interference optics was used to monitor the sedimentation process to reveal the mechanism for the assembly order control (we used the same initial volume fraction in the AUC and PUC experiments so that any effect due to a different volume fraction is ruled out). Figure 2A shows the sedimentation coefficient distribution of SDS-stabilized PS nanoparticles at 15 000 rpm ($g^* \approx 17\,100g$). It shows pronounced "tailing" at a higher s value. Here, s is the sedimentation coefficient which is defined as the ratio of a particle's sedimentation velocity to the applied acceleration causing the sedimentation. The conventional unit is svedberg (Sv) and 1 Sv is equal to 10^{-13} s. The tailing can be resolved into three cluster peaks using the diffusion-corrected $c(s)$ model in the software Sedfit.[26] These three cluster peaks are identified as the dimer, linear trimer, and triangular trimer peaks, respectively, according to their sedimentation coefficients,[27,28] as shown in Table 1. Moreover, by integration of these peaks, the fraction of these clusters was calculated to consist of 3% of the sedimenting particles. In comparison, as shown in Figure 2B, the sedimentation coefficient distribution of charge-stabilized PS nanoparticles shows no tailing at a higher s value and no cluster peaks can be observed using the $c(s)$ model. Overall, as VSANS experiments of the dispersion showed no agglomeration before centrifugation (SI 2) and the AUC experiments indicate the presence of clusters after sedimentation, we conclude that the 3% clusters are most likely formed during the sedimentation process and disturb the crystallization process.[15] In this way, superstructure order control can be achieved by tuning the intensity of an ultracentrifugal field in the easily reachable range from about 17 000 to 154 000g.

Table 1. Sedimentation Coefficients (s Values) of the Monomer and Three Different Clusters, Obtained from Figure 2A[a]

cluster peak	monomer	dimer	trimer 1 (linear)	trimer 2 (triangle)
s value (Sv)	335	570	620	670

[a]The details of the peak assignment are discussed in SI 5.

3.3. Theoretical Calculations. The mechanism of cluster formation was investigated by considering the interparticle interactions in a centrifugal field. The total interparticle potential of the PS nanoparticles (U_{tot}) consists of the electrostatic repulsion (U_R) and the van der Waals attraction (U_A), according to Derjaguin, Landau, Vervey, and Overbeek (DLVO) theory,[29] but here an additional repulsive steric potential U_S due to the presence of surface-bound SDS chains is also present. Therefore,

$$U_{tot} = U_R + U_A + U_S \tag{2}$$

According to the DLVO theory,[30] U_R and U_A can be approximated by eqs 3 and 4

$$U_R = 2\pi\varepsilon_r\varepsilon_0 a\left(\frac{4kT}{ze}\tan h(ze\Psi_0/4kT)\right)^2 \ln[1 + \exp(-\kappa H)] \tag{3}$$

and

$$U_A = -\frac{A}{6}\left(\frac{2a^2}{(2a+H)^2 - 4a^2} + \frac{2a^2}{(2a+H)^2} + \ln\frac{(2a+H)^2 - 4a^2}{(2a+H)^2}\right) \tag{4}$$

U_S can be estimated by using the Alexander-de Gennes polymer brush model,[31−33] which is applicable when $0 < H < 2L$, and given by eq 5

$$U_S = \frac{16kT\pi aL^2\sigma^{3/2}}{35}\left[28\left(\left(\frac{2L}{H}\right)^{1/4} - 1\right) + \frac{20}{11}\left(1 - \left(\frac{H}{2L}\right)^{11/4}\right) + 12\left(\frac{H}{2L} - 1\right)\right] \tag{5}$$

where ε_r is the relative permittivity, ε_0 is the vacuum permittivity, a is the particle radius, Ψ_0 is the surface potential (approximated by the ζ-potential), κ is the reciprocal Debye length, H is the interparticle distance, z is the valency, e is the unit charge, A is the Hamaker constant, σ is the surfactant density on the particle surface, and L is the surfactant chain length.

For PS nanoparticles in water, $\kappa a = 5.2$ and $\Psi_0 \approx \zeta = -40$ mV, and in pH 2 buffer, $\kappa a = 45$ and $\Psi_0 \approx \zeta = -5$ mV. The SDS chain length is ca. 1.2 nm[34] and the surface coverage is ca. 1 SDS per nm^2. The total interparticle potential U_{tot} curves for PS nanoparticles in water and in pH 2 buffer were plotted, as shown in Figures 3A,B, respectively. The energy barrier for coagulation of PS nanoparticles in water is ca. 40 kT, which agrees with the excellent stability and absence of aggregation, as indicated in Figure 2B. Conventional DLVO theory can result in a potential curve with a maximum and a secondary minimum. However, calculating the DLVO curve for PS nanoparticles in pH 2 buffer resulted in a curve showing no maximum and hence no barrier to agglomeration is present, as shown in the red curve in Figure 3B. Adding SDS resulted in steric stabilization with an energy barrier of ca. 6 kT, as indicated by the black curve in Figure 3B. Thus, the dispersion remains monodisperse without any external field (Figure S1–S4). However, in a strong centrifugal field, a small number of clusters were formed, as shown in Figure 2A. The contributing force to overcome the barrier of 6 kT might arise from two sources. First, the particle concentration increases gradually in the sedimentation process, which also contributes to cluster formation since the aggregation rate is proportional to particle concentration.[35] Still another force may come from hydrodynamic interaction. As Folkersma et al.[36] and Xu et al.[37] discussed, hydrodynamic attraction may appear when the particle concentration increases and interparticle distance becomes small. This hydrodynamic attraction can also lead to the formation of clusters. We conclude that with these attractive effects, cluster formation is promoted. The proposed mechanism is plotted schematically in Figure 3C. While without cluster formation, a regular packing occurs (Figure 1A–D), forming a few percent (3%) clusters in an otherwise narrow particle-size distribution (dispersity = 1.07) already

https://doi.org/10.1021/acs.jpcc.1c00143
J. Phys. Chem. C 2021, 125, 8752−8758

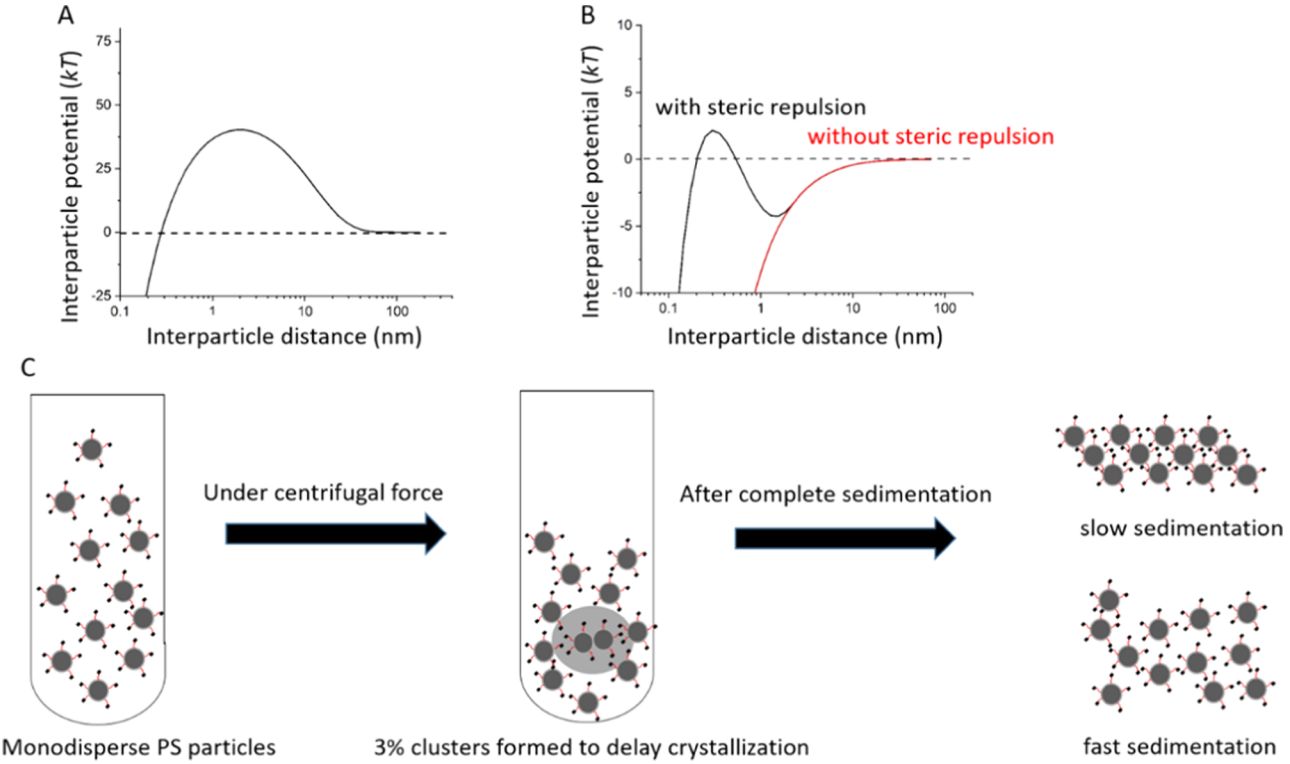

Figure 3. Proposed mechanism behind colloidal assembly order control in preparative ultracentrifugation. The total interparticle potential of SDS-stabilized PS nanoparticles in water is shown in (A) and in pH 2 buffer in (B). A schematic of the mechanism is shown in (C). The red hairs on the surface of particles indicate the surfactant SDS. The hairy structure of the SDS surfactant indicates the stretched-out conformation with the negatively charged head group (dotted end) toward the aqueous phase. Under a sufficiently high centrifugal force, a small number of clusters are formed (highlighted by a gray shade inside the tube). These 3% clusters are formed to disturb the crystallization process and make the superstructure order tunable with the angular velocity: for slow sedimentation, a crystalline structure is formed, while for fast sedimentation, a glassy structure is formed.

induces disorder in particle packings. For a volume fraction of 3%, the average line fraction of such clusters is about $0.03^{1/3} \cong 0.3$. If on a line of unit length, 0.3 is a cluster, the remainder of 0.7 must be occupied with regular particles. As clusters have about the same size as the regular particles, this represents about two particles. Hence, the centers of the clusters have a distance of about 3 particle diameters from each other. From hard sphere packings, it is known that the radial distribution function (RDF) for relatively high density has leveled to about its mean value for a distance corresponding to the fourth coordination shell or after about three-particle diameters.[38] Hence, the presence of 3% clusters is amply sufficient to disturb the packing completely. Obviously, the purely geometric effect is mitigated by the nonhard interactions, but the order of magnitude remains the same.

4. CONCLUSIONS

The assembly of monodisperse colloids at a low Péclet number to a disordered superstructure was shown to be hard in the previous studies,[14,39] especially nanoparticles, mainly due to the intrinsic high diffusion rate of nanoparticles. This work demonstrates that superstructure order from the assembly of nanoparticles can be controlled in ultracentrifugation by simply adjusting the angular velocity. This implies that both ordered and disordered superstructures can be easily obtained by a fast sedimentation method.[40] The mechanism behind this is the introduction of only a tiny amount of clusters (as low as 3%) during the sedimentation, which was detected by the analytical ultracentrifugation. The formation of clusters in sedimentation was further verified by theoretical calculations. The presence of this small amount of clusters slowed down the crystallization rate[15,41] to a level with which the sedimentation rate could compete. In this way, the assembly structure can be simply tuned by changing the angular velocity of preparative ultracentrifugation experiments. Overall, this work provides an easy and versatile approach to construct both crystalline and glassy superstructures from uniformly sized colloids at a low Péclet number, which have a wide application in areas, such as quantum electronics,[42] batteries,[43] and photonic materials. The use of surfactants similar to SDS with varying alkyl chain lengths and the substitution of surfactants with various polyelectrolytes may transform this approach into a general strategy for the fabrication of materials with a tunable degree of order. An especially intriguing next step may be the study of photonic properties of these superstructures with different degrees of order, as both photonic crystals and glasses are proven to be useful in manipulating light.[13,28,44,45] A relationship between different degrees of order of materials and photonic response may be established for tailor-made photonic materials.

■ ASSOCIATED CONTENT

Supporting Information

The Supporting Information is available free of charge at https://pubs.acs.org/doi/10.1021/acs.jpcc.1c00143.

Dynamic light scattering and ζ-potential experiments; very small angle neutron scattering experiments;

https://doi.org/10.1021/acs.jpcc.1c00143
J. Phys. Chem. C 2021, 125, 8752−8758

discussion on size and dispersity obtained from the different techniques; and quantitative analysis of nanoparticle ordering (PDF)

AUTHOR INFORMATION

Corresponding Authors

Helmut Cölfen − *Physical Chemistry, University of Konstanz, 78457 Konstanz, Germany;* orcid.org/0000-0002-1148-0308; Email: helmut.coelfen@uni-konstanz.de

Gijsbertus de With − *Laboratory of Physical Chemistry, Department of Chemical Engineering and Chemistry, Eindhoven University of Technology, 5600MB Eindhoven, the Netherlands;* orcid.org/0000-0002-7163-8429; Email: G.deWith@tue.nl

Authors

Xufeng Xu − *Laboratory of Physical Chemistry, Department of Chemical Engineering and Chemistry, Eindhoven University of Technology, 5600MB Eindhoven, the Netherlands*

Baohu Wu − *Jülich Centre for Neutron Science JCNS at MLZ, Forschungszentrum Jülich, D-85748 Garching, Germany*

Complete contact information is available at: https://pubs.acs.org/10.1021/acs.jpcc.1c00143

Author Contributions

X.X. planned and performed the AUC and PUC experiments under the supervision of G.d.W. and H.C. B.W. performed the SANS experiments. X.X., G.d.W., and H.C. analyzed the data. The manuscript was written through contributions of all authors. All authors have given approval to the final version of the manuscript.

Notes

The authors declare no competing financial interest.

ACKNOWLEDGMENTS

The authors would like to acknowledge the financial support from the EU H2020-MSCA-ITN-2015 project "MULTIMAT" (project number: 676045). The authors would also like to thank Jülich Centre for Neutron Science JCNS at MLZ for VSANS beamtime at KWS-3.

REFERENCES

(1) Lu, Z.; Yin, Y. Colloidal Nanoparticle Clusters: Functional Materials by Design. *Chem. Soc. Rev.* **2012**, *41*, 6874−6887.

(2) Ciesla, U.; Schüth, F. Ordered Mesoporous Materials. *Microporous Mesoporous Mater.* **1999**, *27*, 131−149.

(3) Yang, H.; Xu, Z.; Fan, M.; Gupta, R.; Slimane, R. B.; Bland, A. E.; Wright, I. Progress in Carbon Dioxide Separation and Capture: A Review. *J. Environ. Sci.* **2008**, *20*, 14−27.

(4) Huh, S.; Chen, H.-T.; Wiench, J. W.; Pruski, M.; Lin, V. S. Y. Cooperative Catalysis by General Acid and Base Bifunctionalized Mesoporous Silica Nanospheres. *Angew. Chem., Int. Ed.* **2005**, *44*, 1826−1830.

(5) Lu, S.; Wang, D.; Jiang, S. P.; Xiang, Y.; Lu, J.; Zeng, J. Hpw/Mcm-41 Phosphotungstic Acid/Mesoporous Silica Composites as Novel Proton-Exchange Membranes for Elevated-Temperature Fuel Cells. *Adv. Mater.* **2010**, *22*, 971−976.

(6) Murray, C. B.; Kagan, A. C.; Bawendi, M. Synthesis and Characterization of Monodisperse Nanocrystals and Close-Packed Nanocrystal Assemblies. *Annu. Rev. Mater. Sci.* **2000**, *30*, 545−610.

(7) Boles, M. A.; Engel, M.; Talapin, D. V. Self-Assembly of Colloidal Nanocrystals: From Intricate Structures to Functional Materials. *Chem. Rev.* **2016**, *116*, 11220−11289.

(8) Vogel, N.; Retsch, M.; Fustin, C. A.; Del Campo, A.; Jonas, U. Advances in Colloidal Assembly: The Design of Structure and Hierarchy in Two and Three Dimensions. *Chem. Rev.* **2015**, *115*, 6265−6311.

(9) Chen, M.; Cölfen, H.; Polarz, S. Centrifugal Field-Induced Colloidal Assembly: From Chaos to Order. *ACS Nano* **2015**, *9*, 6944−6950.

(10) Davis, K. E.; Russel, W. B.; Glantschnig, W. J. Disorder-to-Order Transition in Settling Suspensions of Colloidal Silica: X-Ray Measurements. *Science* **1989**, *245*, 507−510.

(11) Whitmer, J. K.; Luijten, E. Sedimentation of Aggregating Colloids. *J. Chem. Phys.* **2011**, *134*, No. 034510.

(12) van Blaaderen, A.; Wiltzius, P. Real-Space Structure of Colloidal Hard-Sphere Glasses. *Science* **1995**, *270*, 1177−1179.

(13) García, P. D.; Sapienza, R.; Blanco, Á.; López, C. Photonic Glass: A Novel Random Material for Light. *Adv. Mater.* **2007**, *19*, 2597−2602.

(14) García, P. D.; Sapienza, R.; López, C. Photonic Glasses: A Step Beyond White Paint. *Adv. Mater.* **2010**, *22*, 12−19.

(15) Auer, S.; Frenkel, D. Suppression of Crystal Nucleation in Polydisperse Colloids Due to Increase of the Surface Free Energy. *Nature* **2001**, *413*, 711.

(16) Royall, C. P.; Vermolen, E. C.; van Blaaderen, A.; Tanaka, H. Controlling Competition between Crystallization and Glass Formation in Binary Colloids with an External Field. *J. Phys.: Condens. Matter* **2008**, *20*, No. 404225.

(17) Schöpe, H. J.; Bryant, G.; van Megen, W. Effect of Polydispersity on the Crystallization Kinetics of Suspensions of Colloidal Hard Spheres When Approaching the Glass Transition. *J. Chem. Phys.* **2007**, *127*, No. 084505.

(18) Turner, S. F.; Clarke, S. M.; Rennie, A. R.; Thirtle, P. N.; Cooke, D. J.; Li, Z. X.; Thomas, R. K. Adsorption of Sodium Dodecyl Sulfate to a Polystyrene/Water Interface Studied by Neutron Reflection and Attenuated Total Reflection Infrared Spectroscopy. *Langmuir* **1999**, *15*, 1017−1023.

(19) Lowry, G. V.; Hill, R. J.; Harper, S.; Rawle, A. F.; Hendren, C. O.; Klaessig, F.; Nobbmann, U.; Sayre, P.; Rumble, J. Guidance to Improve the Scientific Value of Zeta-Potential Measurements in Nanoehs. *Environ. Sci.: Nano* **2016**, *3*, 953−965.

(20) Meconi, G. M.; Ballard, N.; Asua, J. M.; Zangi, R. Adsorption and Desorption Behavior of Ionic and Nonionic Surfactants on Polymer Surfaces. *Soft Matter* **2016**, *12*, 9692−9704.

(21) Piirma, I.; Chen, S.-R. Adsorption of Ionic Surfactants on Latex Particles. *J. Colloid Interface Sci.* **1980**, *74*, 90−102.

(22) Ali, S. I.; Steach, J. C.; Zollars, R. L. Effects of Ionizable Groups on the Adsorption of Surfactants onto Latex Particle Surfaces. *Colloids Surf.* **1987**, *26*, 1−18.

(23) Nodehi, A.; Moosavian, M. A.; Haghighi, M. N.; Sadr, A. A New Method for Determination of the Adsorption Isotherm of SDS on Polystyrene Latex Particles Using Conductometric Titrations. *Chem. Eng. Technol.* **2007**, *30*, 1732−1738.

(24) Bolze, J.; Hörner, K.; Ballauff, M. Competitive Adsorption of an Anionic and a Nonionic Surfactant on Polystyrene Latex Particles as Monitored by Small X-Ray Scattering. *Colloid Polym. Sci.* **1996**, *274*, 1099−1108.

(25) Brown, W.; Zhao, J. Adsorption of Sodium Dodecyl Sulfate on Polystyrene Latex Particles Using Dynamic Light Scattering and Zeta Potential Measurements. *Macromolecules* **1993**, *26*, 2711−2715.

(26) Schuck, P. Size-Distribution Analysis of Macromolecules by Sedimentation Velocity Ultracentrifugation and Lamm Equation Modeling. *Biophys. J.* **2000**, *78*, 1606−1619.

(27) Nieduszynski, I. Dynamic Properties of Biomolecular Assemblies. In *Royal Society of Chemistry*; Harding, Se.; Rowe, A.J., Eds.; Elsevier: Cambridge, 1989; p 374.

(28) Chen, M.; Fischli, D.; Schertel, L.; Aubry, G. J.; Häusele, B.; Polarz, S.; Maret, G.; Cölfen, H. Free-Standing Photonic Glasses Fabricated in a Centrifugal Field. *Small* **2017**, *13*, No. 1701392.

(29) I. Hogg, R.; W. Healy, T.; W. Fuerstenau, D. Mutual Coagulation of Colloid Dispersions. *Trans. Faraday Soc.* **1966**, *62*, 1638−1651.
(30) de With, G. 7. Physical−Chemical Aspects. In *Polymer Coatings*; Wiley-VCH Verlag GmbH & Co.: Weinheim, Germany, 2018.
(31) Alexander, S. Polymer Adsorption on Small Spheres. A Scaling Approach. *J. Phys.* **1977**, *38*, 977−981.
(32) De Gennes, P.-G. Stabilité De Films Polymère/Solvant. *Comptes rendus de l'Académie des sciences. Série 2, Mécanique, Physique, Chimie, Sciences de l'univers, Sciences de la Terre* **1985**, *300*, 839−843.
(33) Kleshchanok, D.; Tuinier, R.; Lang, P. R. Direct Measurements of Polymer-Induced Forces. *J. Phys.: Condens. Matter* **2008**, *20*, No. 073101.
(34) Turner, S.; Clarke, S.; Rennie, A.; Thirtle, P.; Cooke, D.; Li, Z.; Thomas, R. Adsorption of Sodium Dodecyl Sulfate to a Polystyrene/Water Interface Studied by Neutron Reflection and Attenuated Total Reflection Infrared Spectroscopy. *Langmuir* **1999**, *15*, 1017−1023.
(35) Russel, W. B.; Saville, D. A.; Schowalter, W. R. *Colloidal Dispersions*; Cambridge University Press: Cambridge, 1989.
(36) Folkersma, R.; Stein, H.; van de Vosse, F. Hydrodynamic Interactions between Two Identical Spheres Held Fixed Side by Side against a Uniform Stream Directed Perpendicular to the Line Connecting the Spheres' Centres. *Int. J. Multiphase Flow* **2000**, *26*, 877−887.
(37) Xu, W.; Nikolov, A.; Wasan, D. T. The Effect of Many-Body Interactions on the Sedimentation of Monodisperse Particle Dispersions. *J. Colloid Interface Sci.* **1998**, *197*, 160−169.
(38) Solana, J. R., *Perturbation Theories for the Thermodynamic Properties of Fluids and Solids*; CRC Press, 2013.
(39) Jiang, P.; Bertone, J.; Hwang, K. S.; Colvin, V. Single-Crystal Colloidal Multilayers of Controlled Thickness. *Chem. Mater.* **1999**, *11*, 2132−2140.
(40) Pusey, P. N.; van Megen, W. Observation of a Glass Transition in Suspensions of Spherical Colloidal Particles. *Phys. Rev. Lett.* **1987**, *59*, 2083−2086.
(41) Auer, S.; Frenkel, D. Prediction of Absolute Crystal-Nucleation Rate in Hard-Sphere Colloids. *Nature* **2001**, *409*, 1020.
(42) Marcuse, D. *Principles of Quantum Electronics*; Elsevier, 2012.
(43) Balaish, M.; Kraytsberg, A.; Ein-Eli, Y. A Critical Review on Lithium−Air Battery Electrolytes. *Phys. Chem. Chem. Phys.* **2014**, *16*, 2801−2822.
(44) Joannopoulos, J. D.; Villeneuve, P. R.; Fan, S. Photonic Crystals: Putting a New Twist on Light. *Nature* **1997**, *386*, 143.
(45) López, C. Materials Aspects of Photonic Crystals. *Adv. Mater.* **2003**, *15*, 1679−1704.

https://doi.org/10.1021/acs.jpcc.1c00143
J. Phys. Chem. C 2021, 125, 8752−8758